SUPPLEMENTARY INFORMATION

Aqueous alteration of the Vastitas Borealis Formation at the Tianwen-1 landing site

Authors: Changqing Liu,[1] Zongcheng Ling,[1,2]*, Zhongchen Wu,[1] Jiang Zhang,[1] Jian Chen,[1] Xiaohui Fu,[1] Le Qiao,[1] Ping Liu,[1] Bo Li,[1] Li Zhang,[3] Yanqing Xin,[1] Erbin Shi,[1] Haijun Cao,[1] Shangke Tian,[1] Sheng Wan,[1] Hongchun Bai,[1] Jianzhong Liu[4]

***Corresponding author:** Zongcheng Ling, E-mail: zcling@sdu.edu.cn (Z.C. L.)

Affiliations:

1. Shandong Key Laboratory of Optical Astronomy and Solar-Terrestrial Environment, School of Space Science and Physics, Institute of Space Sciences, Shandong University, Weihai 264209, China.

2. CAS Center for Excellence in Comparative Planetology, Chinese Academy of Sciences, Hefei 230026, China.

3. School of Mechanical, Electrical and Information Engineering, Shandong University, Weihai 264209, China

4. Institute of Geochemistry, Chinese Academy of Sciences, Guiyang 550002, China.

Supplementary Notes 1: MarSCoDe Description and Data Acquisition

The MarSCoDe onboard Zhurong rover is a stand-off instrument suite with the capability of determining elemental and mineral compositions at a distance of 1.6 – 7 m. MarsCoDe consists of a Laser-Induced Breakdown Spectrometer (LIBS) to determine elemental compositions and a Short-Wave Infrared Spectrometer (SWIR) to obtain reflectance spectra[1-3].

The LIBS uses a passive Q-switched Nd:YAG laser with a wavelength of 1064 nm, laser energy of 23 mJ per pulse (10 mJ per pulse at 3 m), pulse duration of 4 ns, and repetition rate of 1 – 3 Hz. The output laser is focused on the surface of targets through a beam expander and a telescope. The laser spot size focused on targets varies with different distances, which are 0.06 mm at 1.6 m, 0.11 mm at 3.0 m, 0.18 mm at 5.0 m, and 0.25 mm at 7.0 m. The emission lines from the plasma excited by the laser are collected by the telescope and are transferred into a three-channel spectrometer module with the spectral range of 240 – 340 nm, 340 – 540 nm, and 540 – 850 nm. MarSCoDe carries 12 calibration targets, including six igneous rocks (hypersthene, andesite, olivine, basalt, norite, and K-feldspar), five minerals (nontronite, montmorillonite, dolomite, gypsum, and apatite), and a 6-4 Ti alloy[1]. The Ti alloy plays an important role in on-orbit LIBS wavelength calibration, and the synthetic norite sample is a duplicate of the norite standard carried by ChemCam for cross-calibration between different LIBS instruments[1, 4, 5]. Moreover, the SWIR spectrometer can obtain the reflectance spectra at 800 – 2400 nm with a field of view (FOV, circle region with a diameter of ~58 – 255 mm calculated from the FOV of 36.5 mrad and detection distance[1]) larger than the LIBS laser spot. Two calibration samples of Spectralon reflectance materials are carried by MarSCoDe with the reflectance of 99% (a white piece) and 40% (a gray piece). In addition, a Micro-Imaging camera unit is designed to obtain the texture of Martian targets with a resolution of ≤ 50 μrad per pixel in the pixel area of 1024×1024. The pixel size of the Micro-Imaging camera is calculated from the resolution (≤ 50 μrad per pixel) and varying detection distances (1.8 – 4.2 m), which are 90 – 210 μm.

The level 2B MarSCoDe dataset is published by China National Space Administration (Table S1). Each LIBS spectrum of a single point is averaged from 60 LIBS spectra with an integration time of 1 ms[1], and the emission lines from Martian dust are not removed. The LIBS spectra have been calibrated for wavelength and transformed to absolute radiance ($W \cdot m^{-2} \cdot sr^{-1} \cdot nm^{-1}$). Some LIBS spectra are deserted when the temperature of detectors is lower than 10 °C or higher than 30 °C due to obvious wavelength drift[1, 2]. Finally, 22 LIBS spectra and 22 SWIR spectra are selected (presented in **Table S1**).

Supplementary Notes 2: SDU-LIBS Description and Data Acquisition

The LIBS spectral database at Shandong University (SDU) was collected using the newly built LIBS system plus a Mars chamber in Shandong University at Weihai[6]. 168 terrestrial rocks were ground to powders with grain sizes of <38 μm. Major elemental compositions of these 168 samples were determined by X-ray fluorescence (XRF) on fused glass beads at the State Key Laboratory of ORE Deposit Geochemistry, Chinese Academy of Sciences. The powder of each standard was pressed to a pellet with a diameter of 2 cm. The pressed-pellet samples were placed in a Martian simulation chamber[6, 7], and the LIBS spectra were collected at a distance of ~1.2 m. Three LIBS spectra of each sample were collected from three different locations to avoid the potential inhomogeneity of samples. Ten spectra at each point were collected and averaged, i.e., 30 spectra per sample. Subsequently, the white noise and continuum spectra were respectively removed using wavelet and interpolated spline functions (Fig. S14)[6].

Similar to the spectral conversion from ZR-LIBS to ChemCam, the SDU-LIBS spectra ($\mu W \cdot cm^{-2} nm^{-1}$) are also converted to ChemCam response as mentioned in Methods. In addition, LIBS spectra of four terrestrial targets including argillaceous limestone (GBW07108) and andesite (AGV-2, JA-3, and GBW07104 with distinct chemical compositions) are included in both ChemCam 295 spectra and SDU-LIBS spectral databases, which are selected for cross-calibration between these two LIBS systems.

Supplementary Notes 3: Different Detection Regions by LIBS and SWIR

LIBS and SWIR share different optical paths in MarSCoDe. LIBS used a telescope to collect emission light from plasma excited by a laser, while the reflectance data collected by SWIR does not go through the telescope[1]. Thus, LIBS and SWIR have different detection regions. In particular, LIBS in MarSCoDe can acquire compositions in a depth profile (3.5 mm in soils and 400 μm in rocks for ChemCam[8]) at a submillimeter scale (< 0.2 mm in diameter for MarSCoDe[1]), while SWIR obtains the average reflectance spectra in a circle range with a diameter ~58 – 255 mm and a small penetration depth (~50 μm[9]) due to the scattering of photons on Martian targets. In other words, the detected region and depth of LIBS and SWIR are different although they can point to the same target.

Supplementary Methods: CIPW Norm Calculation Scheme

CIPW norm calculation scheme was designed to estimate modal mineralogy for igneous rocks using major element oxides based on the compositions of saturated normative minerals (e.g., Orthoclase formula of $K_2O \cdot Al_2O_3 \cdot 6SiO_2$), and results are often consistent with the actual mineralogy of the igneous rock from a slowly cooling anhydrous magma[10]. The norm program used in our work has a slight modification compared to the standard CIPW scheme[11], including grouping all plagioclase components as well as combining En, Fs, and Wo into diopside and orthopyroxene.

Supplementary Table 1 The LIBS data files and parameters acquired by ZR-LIBS.

Sample No.	Target description	Sol	Spectral Name	Temperature of Detectors / ℃ Channel 1	Channel 2	Channel 3	Distance / m	Selection
VBF-ZR-01	Indurated soil	21	HX1-Ro_GRAS_MarSCoDe-LIBS-I-05_SCI_N_20210604131244_20210604131304_00021_A.2B	20.6	20.2	20.2	4.0	Y
VBF-ZR-02	Rock	21	HX1-Ro_GRAS_MarSCoDe-LIBS-I-06_SCI_N_20210604132442_20210604132502_00021_A.2B	23.5	23.1	23.5	2.9	Y
VBF-ZR-03	Coarse-grained soil	32	HX1-Ro_GRAS_MarSCoDe-LIBS-I-05_SCI_N_20210615173712_20210615173733_00032_A.2B	10.3	10.3	10.3	3.5	Y
VBF-ZR-04	Rock	32	HX1-Ro_GRAS_MarSCoDe-LIBS-I-06_SCI_N_20210615174910_20210615174931_00032_A.2B	13.7	13.2	13.7	3.4	Y
VBF-ZR-05	Coarse-grained soil	41	HX1-Ro_GRAS_MarSCoDe-LIBS-I-06_SCI_N_20210625034210_20210625034231_00041_A.2B	29.4	29	29.4	4.2	Y
VBF-ZR-06	Coarse-grained soil	41	HX1-Ro_GRAS_MarSCoDe-LIBS-I-07_SCI_N_20210625035429_20210625035450_00041_A.2B	31.7	31.3	31.3	3.4	N
VBF-ZR-07	Layered rock	43	HX1-Ro_GRAS_MarSCoDe-LIBS-I-06_SCI_N_20210626235216_20210626235237_00043_A.2B	5.7	5.1	5.1	4.1	N
VBF-ZR-08	Coarse-grained soil	43	HX1-Ro_GRAS_MarSCoDe-LIBS-I-07_SCI_N_20210627000435_20210627000456_00043_A.2B	8.3	7.8	8.3	3.2	N
VBF-ZR-09	Coarse-grained soil	45	HX1-Ro_GRAS_MarSCoDe-LIBS-I-06_SCI_N_20210629073102_20210629073123_00045_A.2B	27.8	27.4	27.4	3.1	Y
VBF-ZR-10	Coarse-grained soil	45	HX1-Ro_GRAS_MarSCoDe-LIBS-I-07_SCI_N_20210629074321_20210629074342_00045_A.2B	29.4	29	29.4	2.7	Y
VBF-ZR-11	Fine-grained soil	47	HX1-Ro_GRAS_MarSCoDe-LIBS-I-06_SCI_N_20210701022936_20210701022957_00047_A.2B	5.1	5.1	5.1	2.6	N
VBF-ZR-12	Fine-grained soil	47	HX1-Ro_GRAS_MarSCoDe-LIBS-I-07_SCI_N_20210701024155_20210701024216_00047_A.2B	7.8	7.8	7.8	2.3	N
VBF-ZR-13	Coarse-grained soil	50	HX1-Ro_GRAS_MarSCoDe-LIBS-I-06_SCI_N_20210704104745_20210704104806_00050_A.2B	32.1	31.7	32.1	4.2	N
VBF-ZR-14	Coarse-grained soil	50	HX1-Ro_GRAS_MarSCoDe-LIBS-I-07_SCI_N_20210704110004_20210704110025_00050_A.2B	33.6	33.6	33.6	2.7	N
VBF-ZR-15	Coarse-grained soil	58	HX1-Ro_GRAS_MarSCoDe-LIBS-I-07_SCI_N_20210712091310_20210712091331_00058_A.2B	2.9	2.9	2.9	2.9	N
VBF-ZR-16	Coarse-grained soil	58	HX1-Ro_GRAS_MarSCoDe-LIBS-I-08_SCI_N_20210712092659_20210712092720_00058_A.2B	5.7	5.7	5.7	2.9	N
VBF-ZR-17	Coarse-grained soil	65	HX1-Ro_GRAS_MarSCoDe-LIBS-I-06_SCI_N_20210719164325_20210719164346_00065_A.2B	15	14.6	15	3.0	Y
VBF-ZR-18	Coarse-grained soil	65	HX1-Ro_GRAS_MarSCoDe-LIBS-I-07_SCI_N_20210719165714_20210719165735_00065_A.2B	18.1	18.1	18.1	3.0	Y
VBF-ZR-19	Coarse-grained soil	69	HX1-Ro_GRAS_MarSCoDe-LIBS-I-06_SCI_N_20210723192057_20210723192118_00069_A.2B	18.9	18.5	18.9	2.7	Y
VBF-ZR-20	Rock	69	HX1-Ro_GRAS_MarSCoDe-LIBS-I-07_SCI_N_20210723193446_20210723193507_00069_A.2B	22.3	21.8	21.8	2.9	Y
VBF-ZR-21	Layered rock	79	HX1-Ro_GRAS_MarSCoDe-LIBS-I-06_SCI_N_20210803015454_20210803015515_00079_A.2B	18.5	18.5	18.5	1.9	Y
VBF-ZR-22	Rock	79	HX1-Ro_GRAS_MarSCoDe-LIBS-I-07_SCI_N_20210803020843_20210803020904_00079_A.2B	21.8	21.4	21.8	1.8	Y

VBF-ZR-23	Rock	87	HX1-Ro_GRAS_MarSCoDe-LIBS-I-06_SCI_N_20210811071011_20210811071032_00087_A.2B	18.5	18.1	18.5	2.4	Y
VBF-ZR-24	Rock	87	HX1-Ro_GRAS_MarSCoDe-LIBS-I-07_SCI_N_20210811072400_20210811072421_00087_A.2B	21.8	21.4	21.4	3.4	Y
VBF-ZR-25	Fine-grained soil	92	HX1-Ro_GRAS_MarSCoDe-LIBS-I-06_SCI_N_20210816093931_20210816093952_00092_A.2B	12.7	12.3	12.7	2.6	Y
VBF-ZR-26	Fine-grained soil	92	HX1-Ro_GRAS_MarSCoDe-LIBS-I-07_SCI_N_20210816095320_20210816095341_00092_A.2B	15.9	15.9	15.9	3.0	Y
VBF-ZR-27	Rock	100	HX1-Ro_GRAS_MarSCoDe-LIBS-I-06_SCI_N_20210824142112_20210824142133_00100_A.2B	8.9	8.3	8.9	3.3	N
VBF-ZR-28	Coherent rock	100	HX1-Ro_GRAS_MarSCoDe-LIBS-I-07_SCI_N_20210824143501_20210824143522_00100_A.2B	12.3	11.8	11.8	3.1	Y
VBF-ZR-29	Layered rock	103	HX1-Ro_GRAS_MarSCoDe-LIBS-I-06_SCI_N_20210827161232_20210827161253_00103_A.2B	8.3	7.8	7.8	2.8	N
VBF-ZR-30	Coarse-grained soil	103	HX1-Ro_GRAS_MarSCoDe-LIBS-I-07_SCI_N_20210827162621_20210827162642_00103_A.2B	11.8	11.3	11.3	2.5	Y
VBF-ZR-31	Coarse-grained soil	110	HX1-Ro_GRAS_MarSCoDe-LIBS-I-06_SCI_N_20210903204535_20210903204556_00110_A.2B	6.8	6.8	6.8	2.3	N
VBF-ZR-32	Coarse-grained soil	110	HX1-Ro_GRAS_MarSCoDe-LIBS-I-07_SCI_N_20210903205924_20210903205945_00110_A.2B	10.3	9.9	10.3	2.3	Y
VBF-ZR-33	Coarse-grained soil	228	HX1-Ro_GRAS_MarSCoDe-LIBS-I-06_SCI_N_20220103010702_20220103010723_00228_A.2B	2.854	2.258	2.258	2.1	N
VBF-ZR-34	Coarse-grained soil	228	HX1-Ro_GRAS_MarSCoDe-LIBS-I-07_SCI_N_20220103012051_20220103012112_00228_A.2B	5.694	5.694	5.694	2.2	N
VBF-ZR-35	Porous rock	256	HX1-Ro_GRAS_MarSCoDe-LIBS-I-05_SCI_N_20220131193423_20220131193444_00256_A.2B	-1.559	-1.559	-1.559	2.4	N
VBF-ZR-36	Porous rock	256	HX1-Ro_GRAS_MarSCoDe-LIBS-I-06_SCI_N_20220131194812_20220131194833_00256_A.2B	1.652	1.652	1.652	2.4	N
VBF-ZR-37	Porous rock	276	HX1-Ro_GRAS_MarSCoDe-LIBS-I-04_SCI_N_20220221084308_20220221084329_00276_A.2B	-5.142	-5.915	-5.915	3.0	N
VBF-ZR-38	Porous rock	276	HX1-Ro_GRAS_MarSCoDe-LIBS-I-05_SCI_N_20220221085657_20220221085718_00276_A.2B	-2.242	-2.94	-2.242	3.0	N

Note: The six targets emphasized in this study are in bold.

Supplementary Table 2 Absorption features of Martian atmosphere derived from CRISM and ZR-SWIR spectra used for ZR-SWIR wavelength calibration.

CRISM / nm	SWIR / nm	Wavelength shift / nm
1434	1446	12
1954	1964	10
2007	2015	8
2053	2064	11
The average wavelength shift of SWIR		10

Supplementary Table 3 Selected 14 LIBS lines for eight major elements based on the NIST database.

Ion (atom)		**λ / nm**	**Level energy / cm^{-1}**	**Transition**	**Transition probability / s^{-1}**
Si288	Si(I)	288.2	40991.9 – 6298.9	$3s^23p^2$ – $3s^23p4s$	2.17×10^8
Ti335	Ti(I)	335.5	29971.1 – 170.1	$3d^2(^1G)4s4p(^3P°)$ – $3d^24s^2$	6.90×10^7
Al309	Al(I)	309.4	32436.8 – 112.1	$3s^23d$ – $3s^23p$	7.29×10^7
Al394	Al(I)	394.5	25347.8 – 0	$3s^24s$ – $3s^23p$	4.99×10^7
Fe405	Fe(I)	404.7	43079.0 – 18378.2	$3d^6(^3P2)4s4p(^3P°)$ – $3d^64s^2$	2.15×10^5
Fe438	Fe(I)	438.5	47136.1 – 24335.8	$3d^7(^4P)4p$ – $3d^7(^2P)4s$	5.40×10^5
Mg280	Mg(II)	280.3	35669.3 – 0	$2p^63p$ – $2p^63s$	2.57×10^8
Mg448	Mg(II)	448.2	93799.6 – 71491.1	$2p^64f$ – $2p^63d$	2.17×10^8
Ca393	Ca(II)	393.5	25414.4 – 0	$3p^64p$ – $3p^64s$	1.47×10^8
Ca396	Ca(II)	396.9	25191.5 – 0	$3p^64p$ – $3p^64s$	1.40×10^8
Na589	Na(I)	589.2	951390 – 0	$2s^2p^2(^4P)3s$ – $2s^22p3d$	6.14×10^7
Na819	Na(I)	819.1	29172.8 – 16973.4	$2p^63d$ – $2p^63p$	5.14×10^7
K766	K(I)	766.7	13042.9 – 0	$3p^64p$ – $3p^64s$	3.78×10^7
O777	O(I)	777.6	86625.8 – 73768.2	$2s^22p^3(^4S°)3p$ – $2s^22p^3(^4S°)3s$	3.69×10^7

Supplementary Table 4 Root Mean Square Error (RMSE) obtained using the multivariate model built in this study on the LIBS spectra of 295 ChemCam standards, CCCT of ChemCam, 168 SDU-LIBS standards, and the norite cal-target onboard MarSCoDe. The published RMSEs of the ChemCam model, SuperCam model, and MarsCoDe performance test are listed for comparison.

Models and database		**RMSEs / wt.%**							
		SiO_2	**TiO_2**	**Al_2O_3**	**FeO_T**	**MgO**	**CaO**	**Na_2O**	**K_2O**
Multivariate model built in this study	295 ChemCam standards	6.3	0.5	2.9	3.4	1.5	2.2	0.6	0.7
	CCCT	6.0	0.2	1.7	5.1	3.4	3.7	1.0	0.3
	168 SDU-LIBS standards	9.1	0.8	5.1	11.7	2.4	3.9	1.0	1.8
	norite cal-target onboard of ZR-LIBS	7.4	0.2	2.4	8.0	3.3	3.5	0.4	0.1
MarSCoDe Performance test[1]		6.9	–	2.3	–	–	2.0	0.9	0.6
ChemCam model (MOC for test set)[12]		5.3	1.0	3.5	2.3	2.2	2.7	0.6	0.8
SuperCam model[13]		6.1	0.3	1.8	3.1	1.1	1.3	0.5	0.6

Supplementary Table 5 Derived compositions of VBF-ZR targets using the multivariate model built in this study. The RMSEs are listed with the elemental oxides.

Targets	**Sample No.**	**Derived compositions / wt.%**									**CIA / %**
		SiO_2±6	**TiO_2±0.5**	**Al_2O_3±3**	**FeO_T±3**	**MgO±2**	**CaO±2**	**Na_2O±0.6**	**K_2O±0.7**	**Total**	
Indurated soil	**VBF-ZR-01**	59	0.4	15	14	2	11	1.3	0.0	103	39±9
Coarse-grained soil	**VBF-ZR-09**	46	0.8	12	22	6	15	1.7	0.1	103	29±8
Coarse-grained soil	**VBF-ZR-17**	55	2.7	12	15	3	10	2.3	0.7	101	33±10
Fine-grained soil	**VBF-ZR-26**	48	1.5	11	21	6	13	1.7	0.4	102	28±7
Layered rock	**VBF-ZR-21**	42	1.2	13	23	5	16	2.2	1.2	102	28±8
Coherent rock	**VBF-ZR-28**	51	1.5	12	18	3	14	2.0	0.5	102	30±8
Rock	VBF-ZR-02	42	1.7	12	23	5	15	1.6	1.3	102	28±7
Coarse-grained soil	VBF-ZR-03	52	1.7	11	18	4	12	2.2	0.9	102	30±9
Rock	VBF-ZR-04	35	1.3	12	27	8	17	1.3	0.9	102	26±7
Coarse-grained soil	VBF-ZR-05	44	1.3	12	22	5	15	1.9	0.9	102	27±8
Coarse-grained soil	VBF-ZR-10	53	1.7	11	18	4	12	2.5	0.9	102	29±9
Fine-grained soil	VBF-ZR-11	51	2.3	12	18	4	12	2.1	0.7	102	31±9
Fine-grained soil	VBF-ZR-12	44	1.8	11	22	6	14	2.1	0.8	102	27±8
Coarse-grained soil	VBF-ZR-18	44	1.4	11	23	7	15	1.7	0.2	103	26±8
Coarse-grained soil	VBF-ZR-19	41	2.0	13	22	5	15	2.0	1.6	101	29±7
Rock	VBF-ZR-20	41	1.5	11	24	6	15	2.3	1.2	102	25±7
Rock	VBF-ZR-22	50	2.2	9	20	4	13	2.5	0.9	102	25±8
Rock	VBF-ZR-23	48	1.8	11	21	4	14	1.9	1.1	102	26±8

Rock	VBF-ZR-24	48	1.5	11	20	4	13	2.5	1.2	102	28±8
Fine-grained soil	VBF-ZR-25	52	1.5	11	18	4	13	1.7	0.4	102	30±9
Coarse-grained soil	VBF-ZR-30	40	1.5	12	24	7	16	1.5	0.7	102	27±7
Coarse-grained soil	VBF-ZR-32	57	1.5	10	16	3	11	2.1	0.6	102	30±10

FeO_T refers to total iron expressed as the calculated ferrous amount, including both ferric and ferrous.

Supplementary Table 6 The proportions of dust in VBF-ZR soils based on mass-balance analysis. Results of rocks are not provided due to their potential nonuniformity at the scale of laser spot size.

Targets	**Sample No.**	**Mixture ratios / %**		
		VBF-ZR-01	**Dust from Gale crater**	**R^2**
Indurated soil	**VBF-ZR-01**	**100**	**0**	**1.00**
Coarse-grained soil	**VBF-ZR-09**	**18**	**75**	**0.96**
Coarse-grained soil	**VBF-ZR-17**	**75**	**22**	**1.00**
Fine-grained soil	**VBF-ZR-26**	**23**	**73**	**0.98**
Coarse-grained soil	VBF-ZR-03	51	45	0.99
Coarse-grained soil	VBF-ZR-05	17	74	0.94
Coarse-grained soil	VBF-ZR-10	53	45	0.99
Fine-grained soil	VBF-ZR-11	51	45	0.99
Fine-grained soil	VBF-ZR-12	10	81	0.96
Coarse-grained soil	VBF-ZR-18	3	89	0.95
Coarse-grained soil	VBF-ZR-19	12	76	0.92
Fine-grained soil	VBF-ZR-25	53	43	0.99
Coarse-grained soil	VBF-ZR-30	-7	96	0.90
Coarse-grained soil	VBF-ZR-32	72	28	0.99

Supplementary Table 7 Derived chemical compositions of fine-grained soils at Tianwen-1 landing site compared with the published chemical compositions of Martian dust at other landing sites after normalized to the total oxide abundance of eight major elements.

Major elements	SiO_2 / wt.%	TiO_2 / wt.%	Al_2O_3 / wt.%	FeO_T / wt.%	MgO / wt.%	CaO / wt.%	Na_2O / wt.%	K_2O / wt.%	Total / wt.%
ChemCam eolian dust at Gale crater[a14]	48.8	1.2	9.7	22.0	8.5	7.2	2.2	0.4	100.0
Fine-grained soil at Gale crater[b]	42.9±3.7	0.9±0.3	9.2±2.1	18.8±2.2	7.3±1.6	7.2±1.5	2.0±0.6	0.4±0.3	100.0
Gusev Crater dust[c15]	50.1±0.5	1.0±0.08	10.7±0.16	18.4±0.15	9.2±0.15	6.9±0.07	3.2±0.3	0.5±0.07	100.0
Meridiani Planum dust[c16]	50.3±0.3	1.1±0.07	10.2±0.09	19.6±0.04	8.5±0.08	7.3±0.04	2.5±0.19	0.5±0.06	100.0
Average Martian soil[17]	50.1	1.0	10.7	18.5	9.2	7.0	3.0	0.5	100.0
VBF-ZR Fine-grained soil[d]	47.9±6.3	1.8±0.5	11.0±2.9	19.3±3.4	4.9±1.5	12.6±2.2	1.9±0.6	0.6±0.7	100.0

Note: a: compositions of eolian dust derived from the median dust spectrum of 8466 spectra of first shots in sols 1 – 1500.
b: average compositions and standard deviations of fine-grained soils at Gale crater (from PDS Geosciences Node at Washington University in St. Louis)
c: compositions of dust with error values
d: average compositions of VBF-ZR Fine-grained soils (VBF-ZR-11, 12, 25, 26)

Supplementary Table 8 Modal minerals (%) of VBF-ZR targets calculated from CIPW that does not take into account sedimentary processes.

	VBF-ZR-01: Indurated soil	VBF-ZR-09: Coarse soil	VBF-ZR-17: Coarse soil	VBF-ZR-21: Layered rock	VBF-ZR-26: Fine-grained soil	VBF-ZR-28: Coherent rock
Quartz	23.9	0.0	16.9	0.0	0.0	9.3
Plagioclase	41.8	39.7	41.9	24.4	38.0	46.6
Orthoclase	0.0	0.0	6.5	0.0	3.2	0.0
Nepheline	0.0	4.6	0.0	14.9	0.0	0.0
Diopside	24.6	37.5	21.4	24.9	38.6	32.0
Hypersthene	7.7	0.0	8.3	0.0	7.6	8.4
Olivine	0.0	14.1	0.0	16.2	7.7	0.0
Ilmenite	0.4	1.1	3.2	2.2	2.0	1.6
Magnetite	1.7	2.9	1.9	3.1	2.9	2.2
Other minerals	0.0	0.0	0.0	14.2	0.0	0.0

Supplementary Table 9 Comparison of the elemental compositions at Tianwen-1 landing site derived from ZR-LIBS data, compared with the published result of GRS from the same area (5°×5°, from PDS Geosciences Node at Washington University in St. Louis).

Database	**SiO_2 / wt.%**	**FeO_T / wt.%**	**FeO_T/SiO_2**	**K_2O / wt.%**	**Na_2O / wt.%**	**Na_2O/ K_2O***
MarSCoDe[a]	47.5±6.0	20.4±3.0	0.43	0.8±0.4	2.0±0.3	2.5
GRS[b]	42.9±1.3	17.8±1.4	0.41	0.6±0.04	1.5*	

* = calculated using average Na_2O/ K_2O of MarSCoDe results of 22 VBF-ZR targets

a: average compositions ± standard deviation of 22 VBF-ZR targets

b: compositions ± errors from PDS Geosciences Node at Washington University in St. Louis and Boynton et al., (2007)[18] Supplementary Table 10 List of spectral files of the norite cal-target obtained by ZR-LIBS and ChemCam on Mars.

ID	LIBS payloads	Spectral name
01	ZR-LIBS	HX1-Ro_GRAS_MarSCoDe-LIBS-I-02_CAL_N_20210625031654_20210625031715_00041_A.2B
02	ZR-LIBS	HX1-Ro_GRAS_MarSCoDe-LIBS-I-02_CAL_N_20210803012830_20210803012851_00079_A.2B
03	ChemCam	CL5_399890138CCS_F0030530CCAM01027P3.CSV
04	ChemCam	CL5_404237967CCS_F0050104CCAM01076P3.CSV
05	ChemCam	CL5_407435130CCS_F0050432CCAM02112P3.CSV
06	ChemCam	CL5_409386579CCS_F0051858CCAM02134P3.CSV
07	ChemCam	CL5_411084120CCS_F0051954CCAM02153P3.CSV
08	ChemCam	CL5_414538232CCS_F0060000CCAM03192P3.CSV
09	ChemCam	CL5_424845745CCS_F0060646CCAM02308P3.CSV
10	ChemCam	CL5_426784925CCS_F0070270CCAM01330P3.CSV
11	ChemCam	CL5_426786009CCS_F0070270CCAM02330P3.CSV
12	ChemCam	CL5_428738487CCS_F0110302CCAM03352P3.CSV
13	ChemCam	CL5_428738552CCS_F0110302CCAM03352P3.CSV
14	ChemCam	CL5_428738616CCS_F0110302CCAM03352P3.CSV
15	ChemCam	CL5_428738720CCS_F0110302CCAM03352P3.CSV
16	ChemCam	CL5_428738783CCS_F0110302CCAM03352P3.CSV
17	ChemCam	CL5_428738847CCS_F0110302CCAM03352P3.CSV
18	ChemCam	CL5_428738956CCS_F0110302CCAM03352P3.CSV
19	ChemCam	CL5_428739020CCS_F0110302CCAM03352P3.CSV
20	ChemCam	CL5_428739084CCS_F0110302CCAM03352P3.CSV
21	ChemCam	CL5_429182799CCS_F0110748CCAM03357P3.CSV
22	ChemCam	CL5_429182964CCS_F0110748CCAM03357P3.CSV
23	ChemCam	CL5_429183028CCS_F0110748CCAM03357P3.CSV
24	ChemCam	CL5_429183142CCS_F0110748CCAM03357P3.CSV
25	ChemCam	CL5_429183206CCS_F0110748CCAM03357P3.CSV
26	ChemCam	CL5_429183269CCS_F0110748CCAM03357P3.CSV
27	ChemCam	CL5_429183374CCS_F0110748CCAM03357P3.CSV
28	ChemCam	CL5_429183438CCS_F0110748CCAM03357P3.CSV
29	ChemCam	CL5_429183502CCS_F0110748CCAM03357P3.CSV
30	ChemCam	CL5_432199003CCS_F0160000CCAM01391P3.CSV
31	ChemCam	CL5_493729689CCS_F0491420CCAM05082P3.CSV
32	ChemCam	CL5_512100457CCS_F0532298CCAM06291P3.CSV
33	ChemCam	CL5_564214170CCS_F0670000CCAM03877P3.CSV
34	ChemCam	CL5_577176687CCS_F0691858CCAM05022P3.CSV
35	ChemCam	CL5_582953916CCS_F0710228CCAM06088P3.CSV
36	ChemCam	CL5_587823134CCS_F0721316CCAM07143P3.CSV
37	ChemCam	CL5_602114094CCS_F0732394CCAM04304P3.CSV
38	ChemCam	CL5_606380414CCS_F0750264CCAM06352P3.CSV
39	ChemCam	CL5_616503609CCS_F0762080CCAM04465P3.CSV

40	ChemCam	CL5_622016633CCS_F0763002CCAM01529P3.CSV
41	ChemCam	CL5_627342282CCS_F0772038CCAM04587P3.CSV
42	ChemCam	CL5_632398655CCS_F0781652CCAM03645P3.CSV
43	ChemCam	CL5_640392072CCS_F0791222CCAM03735P3.CSV

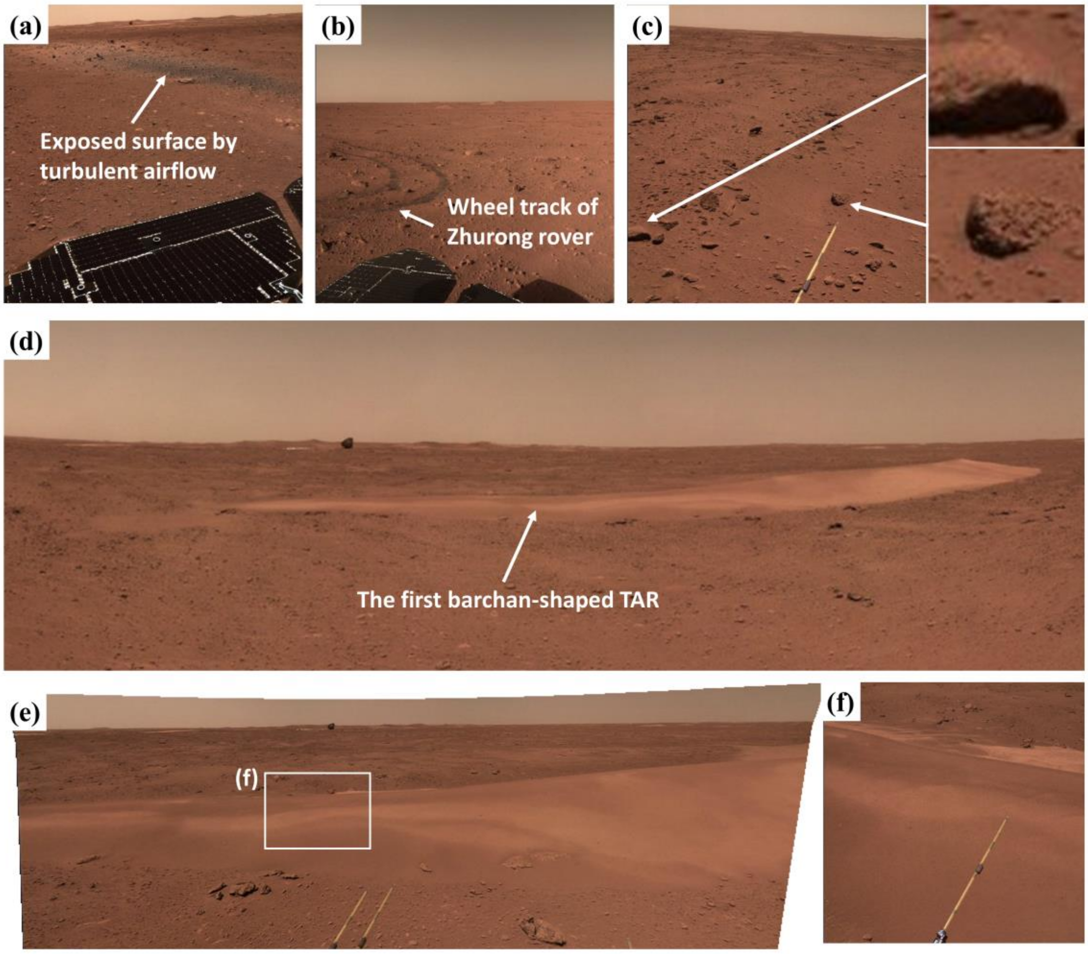

Supplementary Figure 1 Local contexts and TAR1 along the Zhurong rover traverse acquired by the Navigation and Topography Camera (NaTeCam) provided by China National Space Administration. (a) the exposed dark-toned surface with the dust removed by the turbulent airflow during landing. (b) wheel track of Zhurong rover reveals the dark-toned materials. (c) image and close-up images of rocks showing layered structures and spaced pits on the surface. (d – f) images of the first TAR. It's a barchan-shaped TAR with intermittent distribution of dark and bright sand. The white square in (e) represents the detection region of (f).

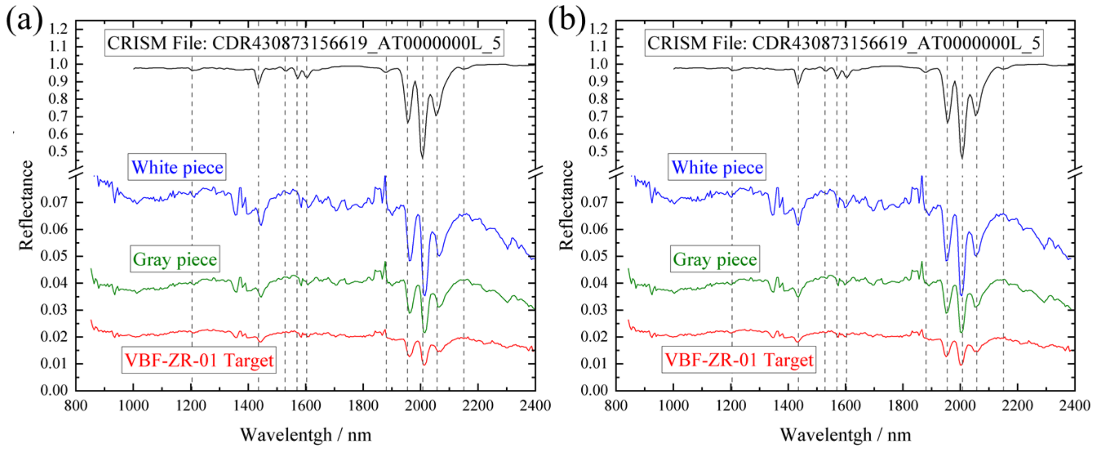

Supplementary Figure 2 SWIR spectra before (a) and after (b) wavelength calibration using absorption features of the Martian atmosphere (Table S2). SWIR radiance of the indurated soil (VBF-ZR-01) and the white and gray pieces of cal-target are converted into reflectance by dividing the solar spectrum provided by Gueymard (2004)[19]. Absorption features of Martian atmosphere were obtained from the CRISM Analysis Toolkit (CAT)[20].

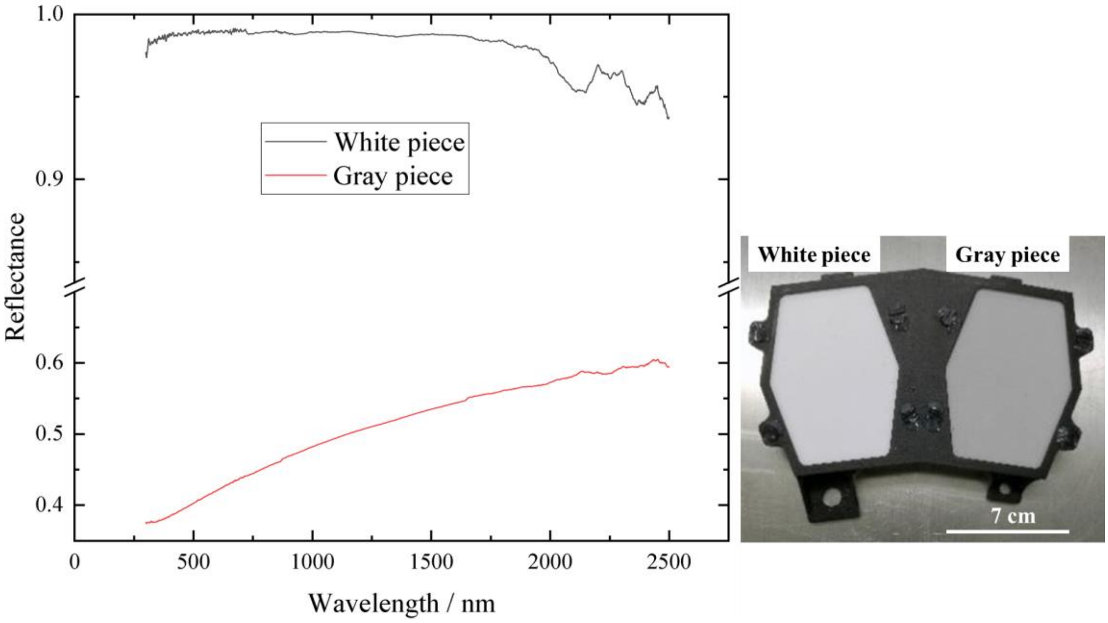

Supplementary Figure 3 Absolute reflectance spectra of SWIR calibration targets (white and gray pieces).

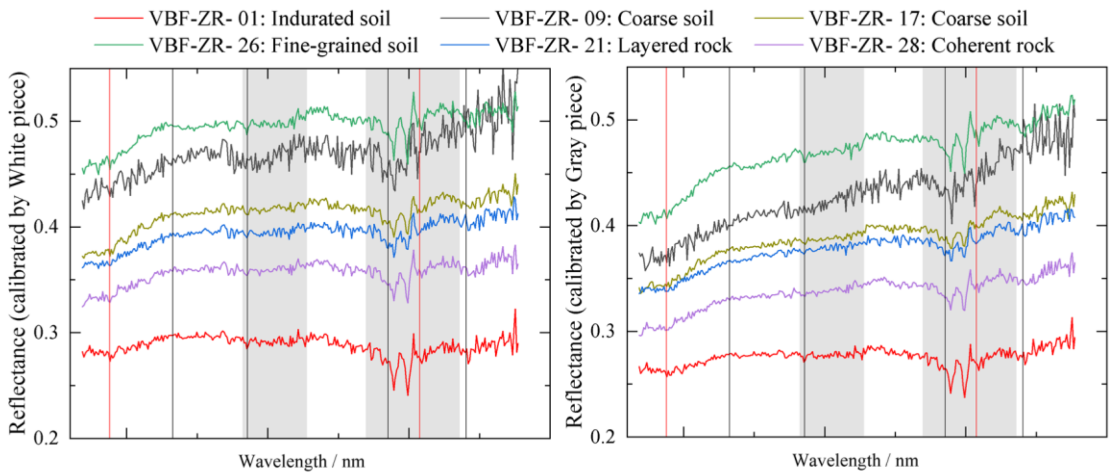

Supplementary Figure 4 SWIR spectra of selected VBF-ZR targets calibrated using the white and gray calibration targets, which show similar absorption features.

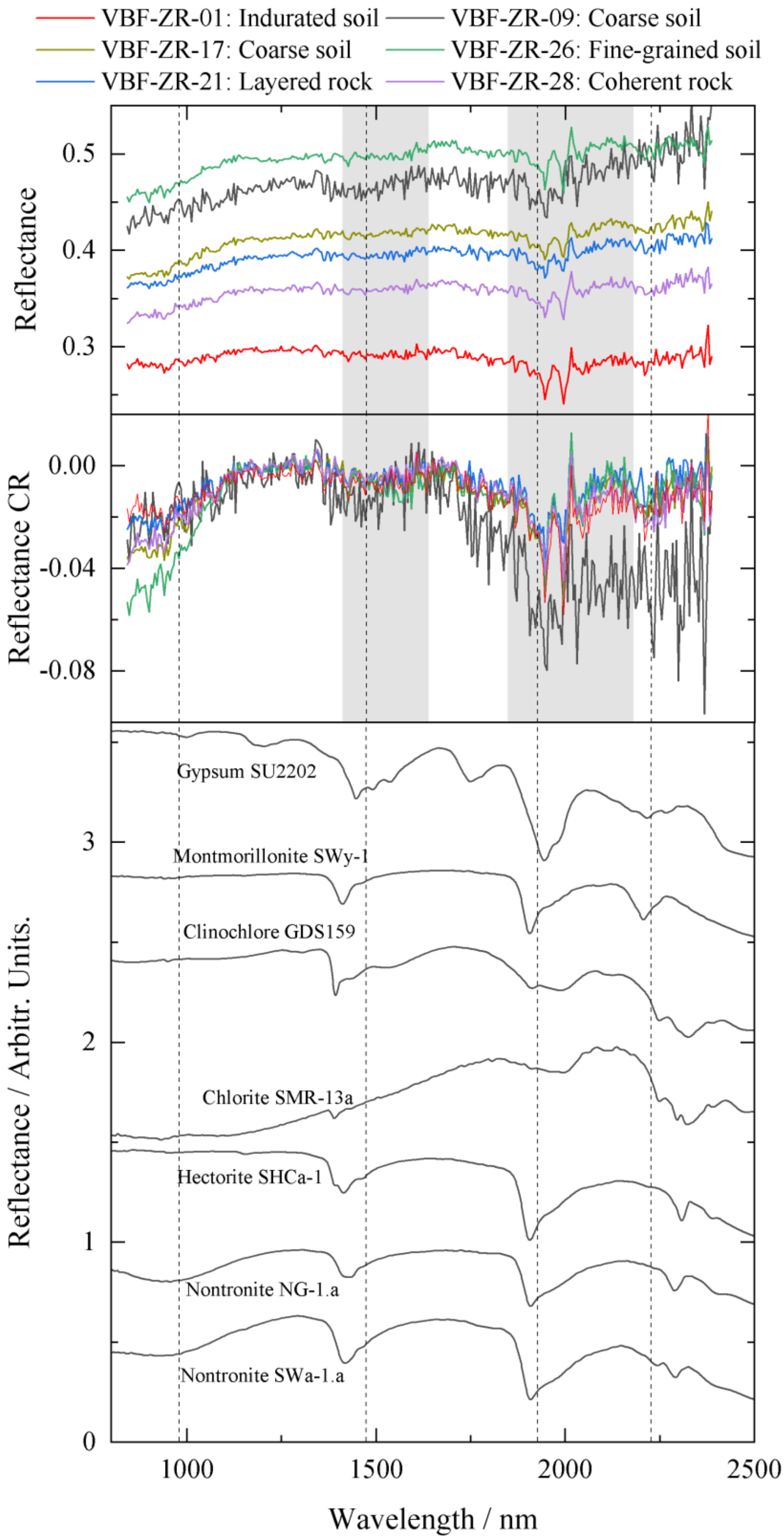

Supplementary Figure 5 SWIR spectra of selected VBF-ZR targets. (a – b) Absolute reflectance spectra before and after continuum removal (CR). (c) Spectra of nontronite (SWa-1a and NG-1a), hectorite (SHCa-1), chlorite (SMR-13a), clinochlore (GDS159), montmorillonite (SWy-1), and gypsum (SU2202) from USGS database[21]. Dotted lines indicate the absorption centers of SWIR spectra.

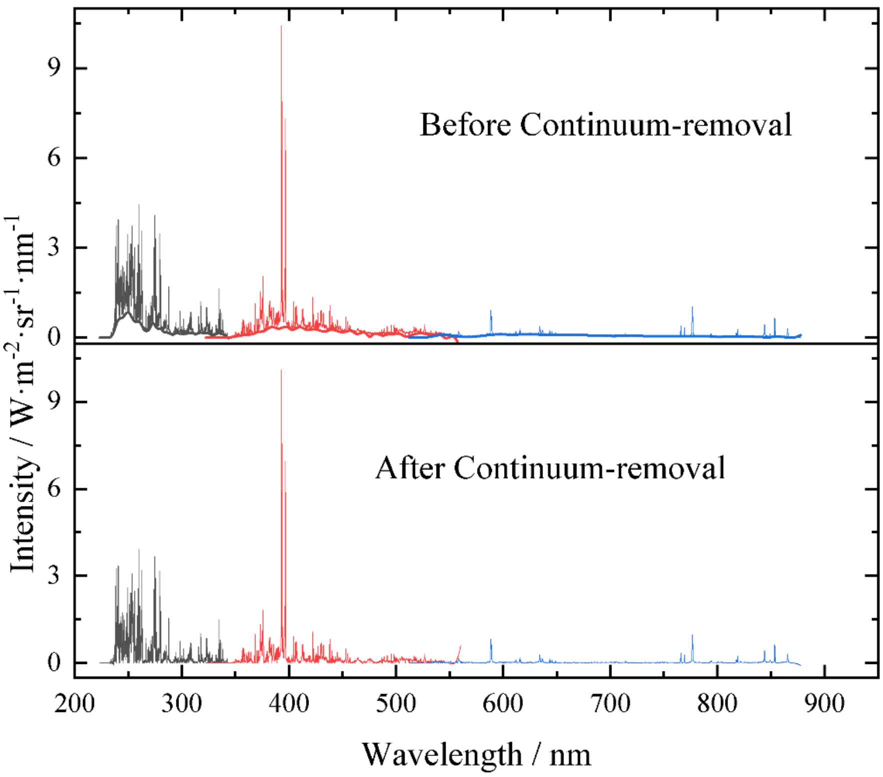

Supplementary Figure 6 The pre-processed LIBS spectrum of No.17 acquired by ZR-LIBS.

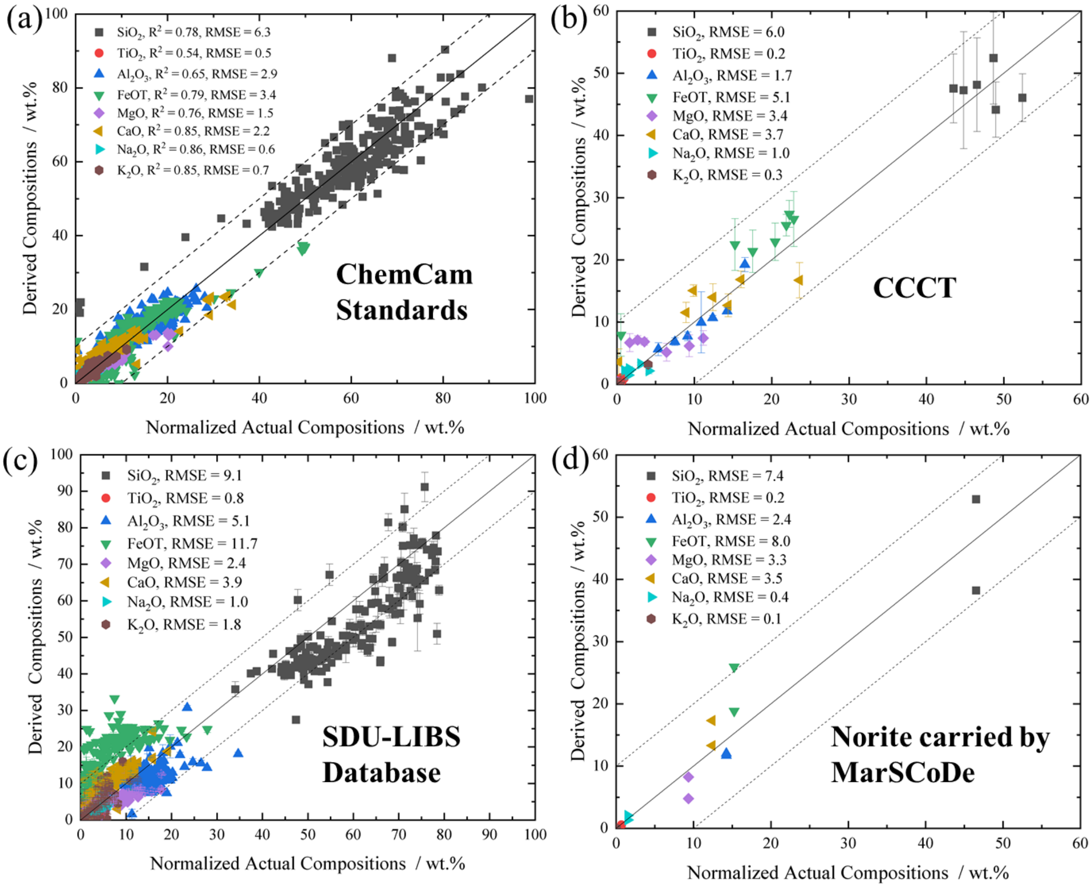

Supplementary Figure 7 Actual and derived element compositions using our multivariate model for 295 ChemCam standards (a), CCCT (b), 168 SDU-LIBS standards (c), and norite carried by MarSCoDe (d). The straight line indicates the 1:1 line, and the dotted lines indicate a buffer zone of ±10 wt. %. The error bars are standard deviation of derived chemical compositions.

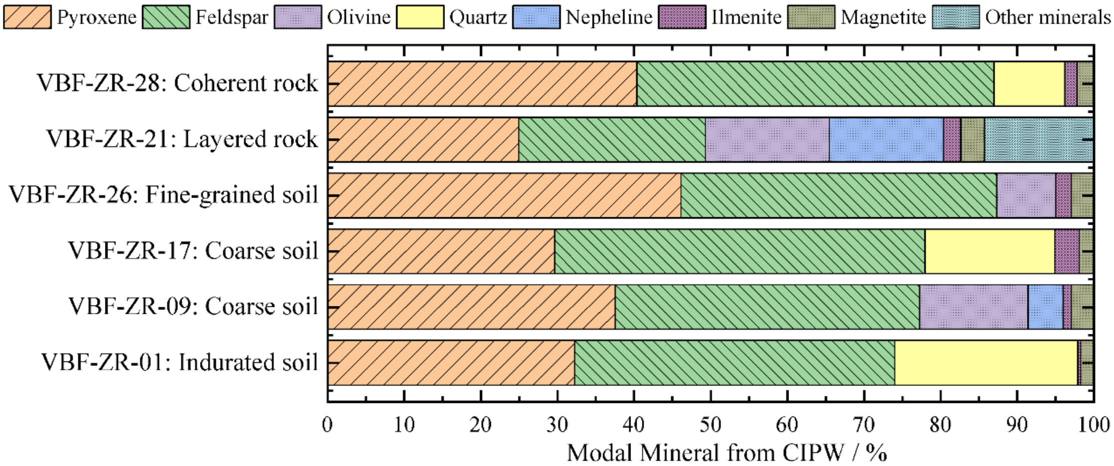

Supplementary Figure 8 Modal minerals of VBF-ZR targets calculated from CIPW that does not take into account sedimentary processes.

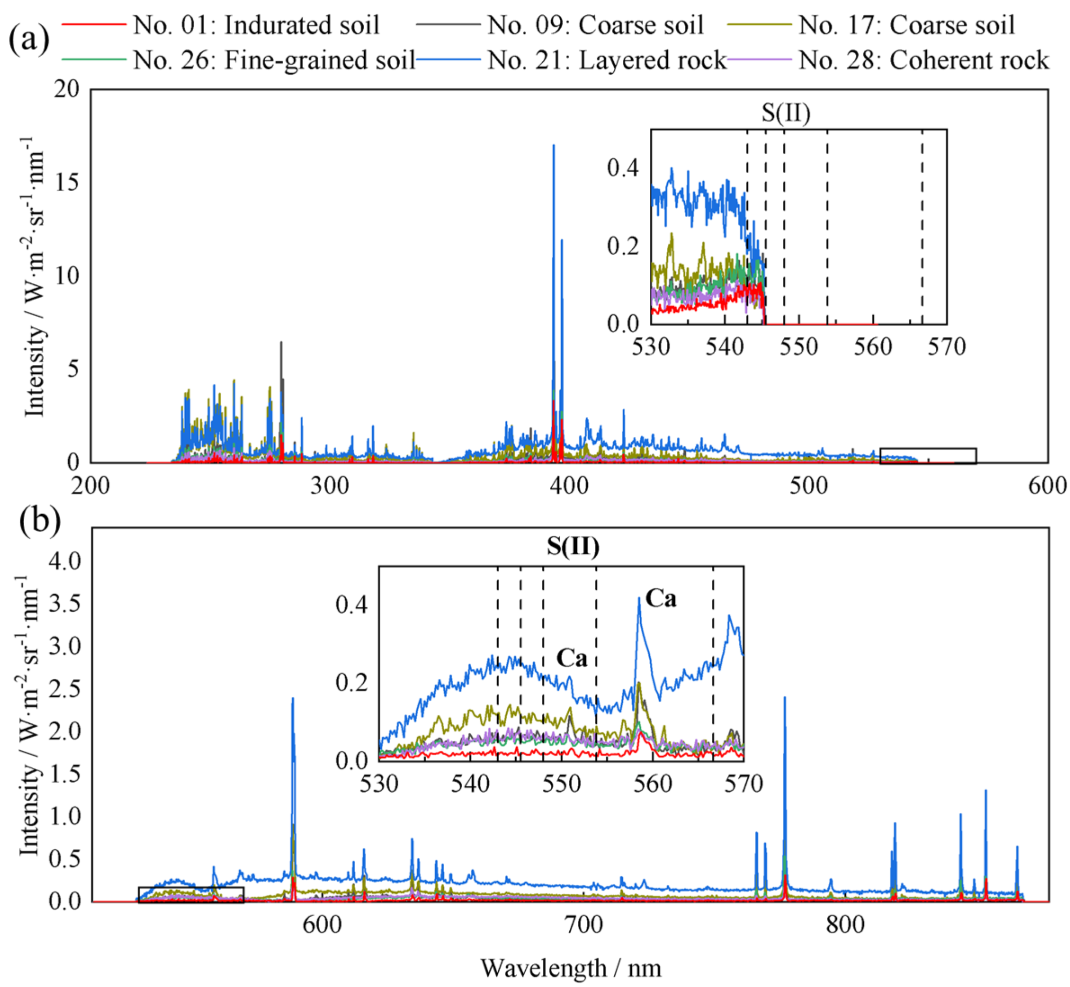

Supplementary Figure 9 LIBS spectra of six selected VBF-ZR targes before pre-processing with the wavelength of sulfur emissions at 543.0 nm, 545.5 nm, 548.0 nm, 553.8 nm and 566.6 nm from NIST database[22]. (a) LIBS spectra collected by the first two spectrometers (240 – 540 nm). (b) spectra collected by the third spectrometer (540 – 850 nm).

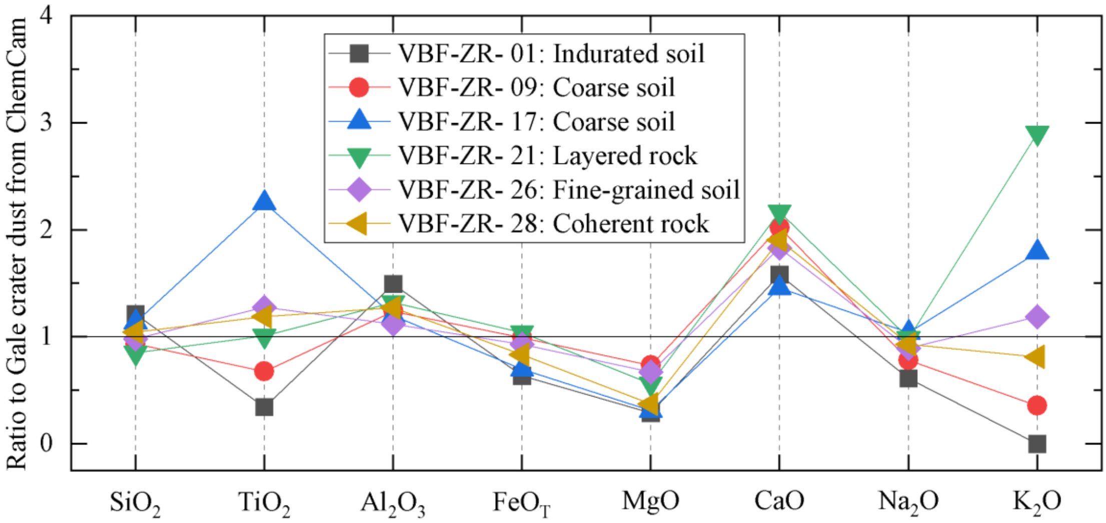

Supplementary Figure 10 Relative concentrations of eight major elements of VBF-ZR targets normalized to the Mars global dust compositions derived from ChemCam data (data in Table S7).

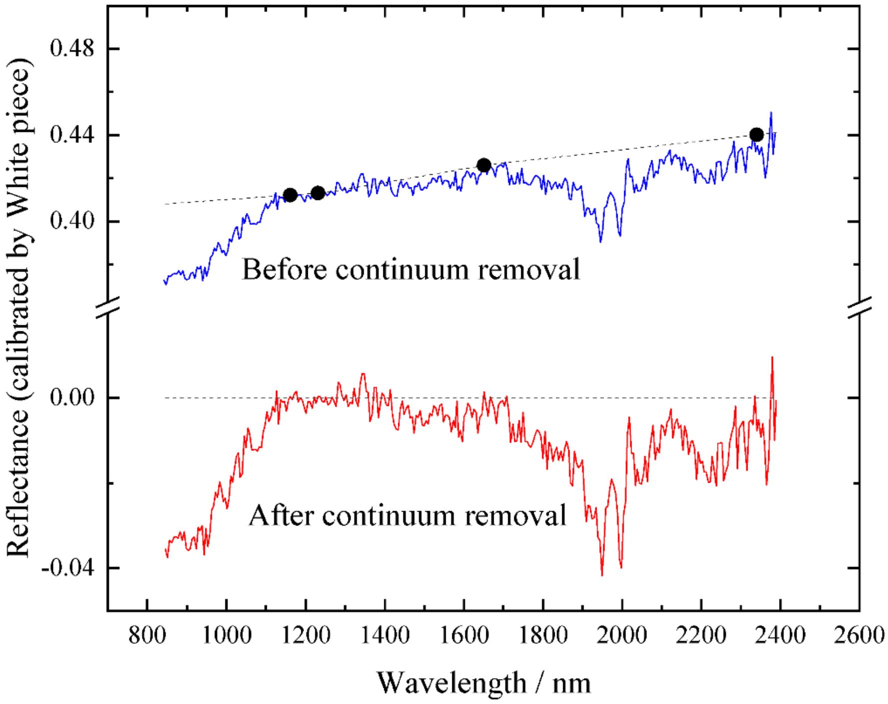

180
181
182 Supplementary Figure 11 SWIR reflectance spectra of coarse soil (VBF-ZR-17) before and after
183 continuum removal.
184

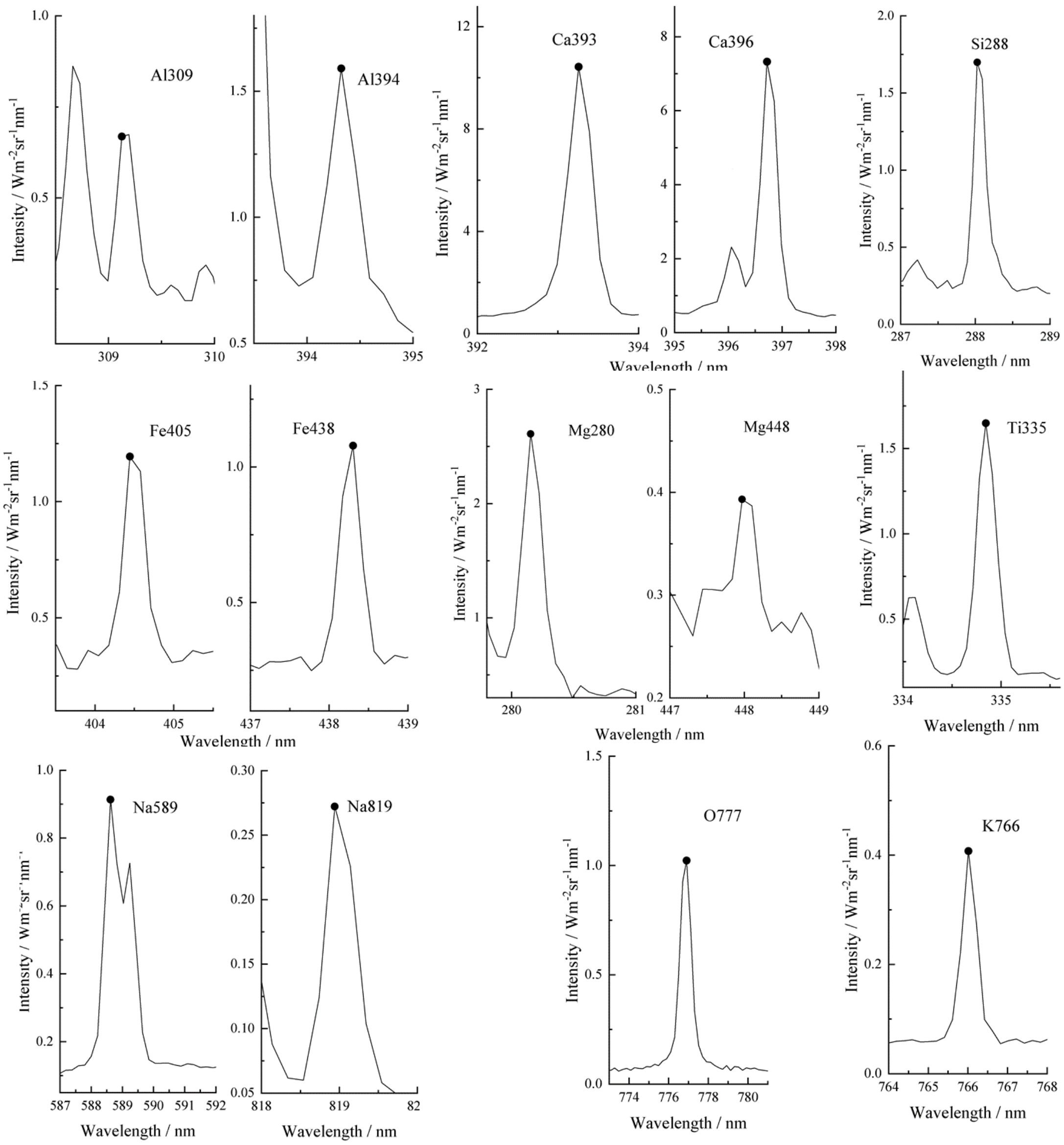

Supplementary Figure 12 Selected 14 emission lines of nine major elements for the ZR-LIBS spectrum of coarse soil (VBF-ZR-17).

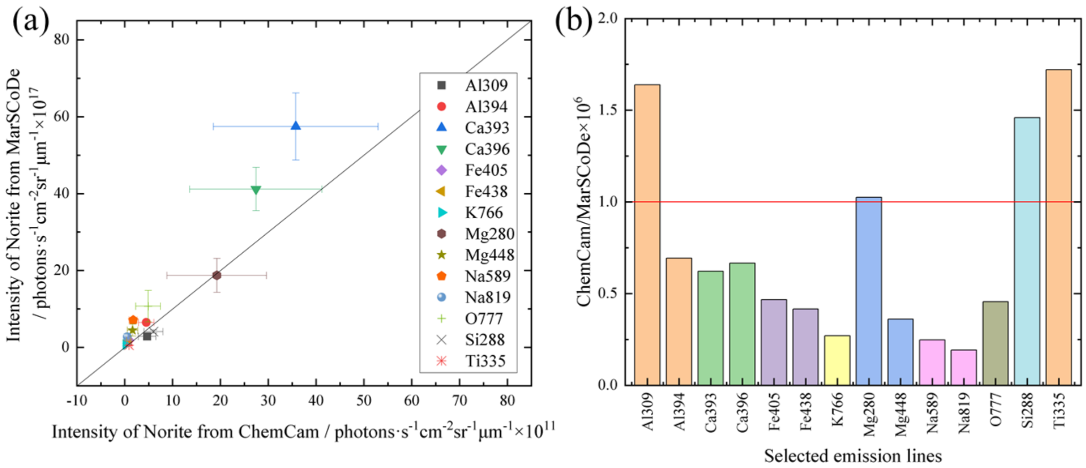

Supplementary Figure 13 The intensity (a) and intensity ratios (b) of selected 14 emission lines from the norite cal-target acquired by MarSCoDe and by ChemCam after radiance transformation. The intensity of ZR-LIBS emission lines is six orders of magnitude higher than those of the ChemCam spectrum although they have the same unit of photons·s^{-1}cm^{-2}sr^{-1}μm^{-1}. The error bars are standard deviation of the emission line intensities from all ChemCam-Norite and MarSCoDe-Norite.

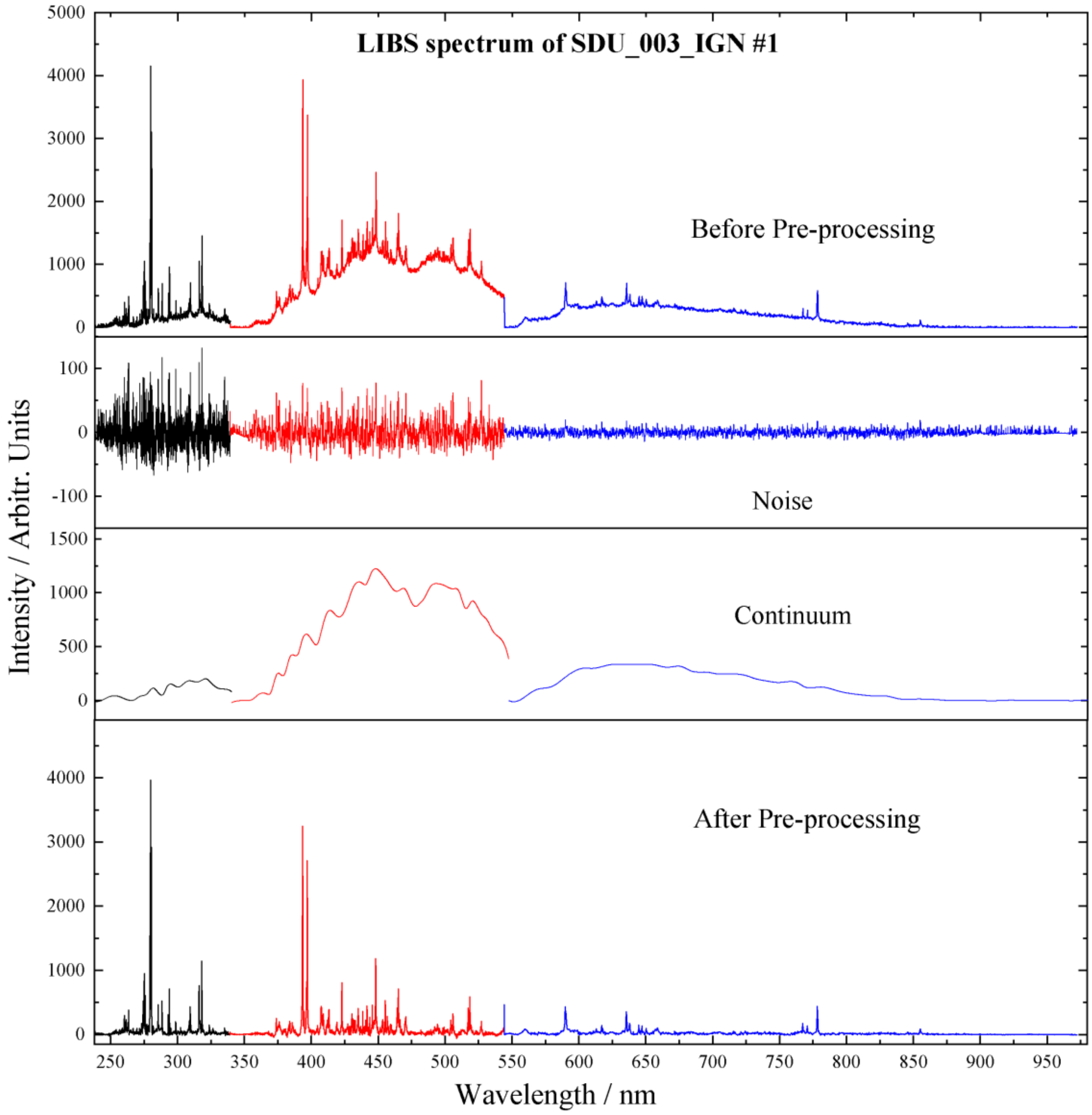

Supplementary Figure 14 LIBS spectrum of SDU_003_IGN (augite) collected by SDU-LIBS before and after the noise and continuum removal.

Supplementary References

1. Xu W, Liu X, Yan Z, Li L, Zhang Z, Kuang Y, *et al.* The MarSCoDe Instrument Suite on the Mars Rover of China's Tianwen-1 Mission. *Space Science Reviews* 2021, **217**(5)**:** 1-58.
2. Wan X, Yuan R, Wang H, Cheng Y, Jia J, Shu R, *et al.* Elastic Particle Swarm Optimization for MarSCoDe Spectral Calibration on Tianwen-1 Mars Rover. *Analytical Chemistry* 2021, **93**(22)**:** 7970-7977.
3. Zou Y, Zhu Y, Bai Y, Wang L, Jia Y, Shen W, *et al.* Scientific objectives and payloads of Tianwen-1, China's first Mars exploration mission. *Advances in Space Research* 2021, **67**(2)**:** 812-823.
4. Fabre C, Maurice S, Cousin A, Wiens R, Forni O, Sautter V, *et al.* Onboard calibration igneous targets for the Mars Science Laboratory Curiosity rover and the Chemistry Camera laser induced breakdown spectroscopy instrument. *Spectrochimica Acta Part B: Atomic Spectroscopy* 2011, **66**(3-4)**:** 280-289.
5. Wiens RC, Maurice S, Barraclough B, Saccoccio M, Barkley WC, Bell JF, *et al.* The ChemCam instrument suite on the Mars Science Laboratory (MSL) rover: Body unit and combined system tests. *Space science reviews* 2012, **170**(1)**:** 167-227.
6. Liu C, Ling Z, Zhang J, Wu Z, Bai H, Liu Y. A Stand-Off Laser-Induced Breakdown Spectroscopy (LIBS) System Applicable for Martian Rocks Studies. *Remote Sensing* 2021, **13**(23)**:** 4773.
7. Wu Z, Ling Z, Zhang J, Fu X, Liu C, Xin Y, *et al.* A Mars Environment Chamber Coupled with Multiple In Situ Spectral Sensors for Mars Exploration. *Sensors* 2021, **21**(7)**:** 2519.
8. Maurice S, Clegg SM, Wiens RC, Gasnault O, Rapin W, Forni O, *et al.* ChemCam activities and discoveries during the nominal mission of the Mars Science Laboratory in Gale crater, Mars. *Journal of Analytical Atomic Spectrometry* 2016, **31**(4)**:** 863-889.
9. Clarke FC, Hammond SV, Jee RD, Moffat AC. Determination of the information depth and sample size for the analysis of pharmaceutical materials using reflectance near-infrared microscopy. *Applied spectroscopy* 2002, **56**(11)**:** 1475-1483.
10. Kelsey C. Calculation of the CIPW norm. *Mineralogical magazine journal of the Mineralogical Society* 1965, **34**(268)**:** 276-282.
11. Hollocher K. CIPW norm calculation program. *Geology Department, Union College* 2004.
12. Clegg SM, Wiens RC, Anderson R, Forni O, Frydenvang J, Lasue J, *et al.* Recalibration of the Mars Science Laboratory ChemCam instrument with an expanded geochemical database. *Spectrochimica Acta Part B-Atomic Spectroscopy* 2017, **129:** 64-85.
13. Anderson RB, Forni O, Cousin A, Wiens RC, Clegg SM, Frydenvang J, *et al.* Post-landing major element quantification using SuperCam laser induced breakdown spectroscopy. *Spectrochimica Acta Part B: Atomic Spectroscopy* 2021**:** 106347.
14. Lasue J, Cousin A, Meslin PY, Mangold N, Wiens RC, Berger G, *et al.* Martian eolian dust probed by ChemCam. *Geophysical Research Letters* 2018, **45**(20)**:** 10,968-910,977.
15. Gellert R, Rieder R, Brückner J, Clark B, Dreibus G, Klingelhöfer G, *et al.* Alpha Particle X-ray Spectrometer (APXS): Results from Gusev crater and calibration report. *Journal of Geophysical Research: Planets* 2006, **111**(E2).
16. Morris RV, Klingelhoefer G, Schröder C, Rodionov DS, Yen A, Ming DW, *et al.* Mössbauer

mineralogy of rock, soil, and dust at Meridiani Planum, Mars: Opportunity's journey across sulfate-rich outcrop, basaltic sand and dust, and hematite lag deposits. *Journal of Geophysical Research: Planets* 2006, **111**(E12).

17. Taylor SR, McLennan S. *Planetary crusts: their composition, origin and evolution*, vol. 10. Cambridge University Press, 2009.
18. Boynton W, Taylor G, Evans LG, Reedy R, Starr R, Janes D, *et al.* Concentration of H, Si, Cl, K, Fe, and Th in the low-and mid-latitude regions of Mars. *Journal of Geophysical Research: Planets* 2007, **112**(E12).
19. Gueymard CA. The sun's total and spectral irradiance for solar energy applications and solar radiation models. *Solar energy* 2004, **76**(4)**:** 423-453.
20. Viviano-Beck CE, Seelos FP, Murchie SL, Kahn EG, Seelos KD, Taylor HW, *et al.* Revised CRISM spectral parameters and summary products based on the currently detected mineral diversity on Mars. *Journal of Geophysical Research: Planets* 2014, **119**(6)**:** 1403-1431.
21. Clark RN, Swayze GA, Wise RA, Livo KE, Hoefen TM, Kokaly RF, *et al.* USGS digital spectral library splib06a: US Geological Survey; 2007. Report No.: 2327-638X.
22. Kramida A, Ralchenko Y, Reader J, (2020) NAT. NIST Atomic Spectra Database (ver. 5.8), [Online]. Gaithersburg: National Institute of Standards and Technology; 2021.